Enhanced magnetoresistance of $La_{2/3}Ca_{1/3}MnO_3/CeO_2$ nanocystalline composites synthesized by polymer-network gel method

L. D. Yao and W. Zhang
Beijing National Laboratory for Condensed Matter Physics, Institute of Physics, Chinese Academy of Sciences, P.O. Box 603, Beijing 100080, People's Republic of China

J. S. Zhang
Department of Chemistry, Anyang Normal University, Anyang 455002, People's Republic of China

H. Yang, F. Y. Li, Z. X. Liu, C. Q. Jin, and R. C. Yu[a)]
Beijing National Laboratory for Condensed Matter Physics, Institute of Physics, Chinese Academy of Sciences, P.O. Box 603, Beijing 100080, People's Republic of China

(Received 13 December 2006; accepted 19 January 2007; published online 21 March 2007)

Using a dispersing particle polymer-network gel method, we prepared $x La_{2/3}Ca_{1/3}MnO_3/(1-x)CeO_2$ nanocystalline composites, where the average grain sizes of $La_{2/3}Ca_{1/3}MnO_3$ and CeO_2 are about 30 nm and less than 10 nm, respectively. The magnetoresistance of the sintered composites is explored as a function of the ratio of metal/insulator, temperature, and magnetic field. The system exhibits metallic percolation threshold at $x=x_p \sim 35\%$, around which the high field magnetoresistance has a maximum ($\sim 70\%$) at 50 K and 5 T, and the low field magnetoresistance value is close to 16% at 5 K and 0.05 T. © *2007 American Institute of Physics*.
[DOI: 10.1063/1.2712178]

I. INTRODUCTION

Mixed-valence manganese perovskites of the form $A_{1-x}B_xMnO_3$ (A=La, Nd, Pr, etc., a trivalent rare earth, and B=Ca, Sr, Ba, etc., a divalent element) have been intensively studied since the discovery of the colossal magnetoresistance effect (CMR) in the 1980's.[1–3] The so-called CMR related to double exchange interaction is viewed as an intrinsic property of manganite materials. Typically, for a single-crystal manganite, such as $La_{2/3}Ca_{1/3}MnO_3$ (LCMO), the decrease in resistance occurs around the Curie temperature (T_C) under external magnetic fields.[4,5] However, it is difficult to apply to electronic devices because the CMR effect is restricted to a narrow range of temperature near the T_C and a large external magnetic field. Some experimentalists and theoreticians have still made great efforts in trying to improve the electrical and magnetic properties of this kind of compound for potential industrial uses and discovered another type of magnetoresistance (MR), intergranular MR,[6] which is related to spin-polarized tunneling through the insulating grain boundaries in polycrystalline or fine particle systems. It was reported that the great MR values lies in the almost complete spin polarization.[6–8] The extrinsic MR phenomenon was first reported in the polycrystalline $La_{2/3}Sr_{1/3}MnO_3$ by Hwang *et al.*[6] The extreme sensitivity of ferromagnetic (FM) interaction to interfaces roots in insulatinglike barriers at grain boundaries in this polycrystalline materials. Thus, the nearly complete spin polarization[9] below the ferromagnetic transition temperature can also be utilized in the form of spin-polarized tunneling through CMR/insulator/CMR junctions, since the junctions can act as the natural grain boundaries. In order to increase boundary effects, some nanocrystalline materials were prepared by the sol-gel technique.[10,11] In addition, the artificial grain boundaries[12,13] are also added by making CMR-insulator composites, where the boundaries to FM interaction is similar to that of natural ones. Towards the end $La_{0.7}Sr_{0.3}MnO_3$/glass composites,[14] $La_{0.67}Ca_{0.33}MnO_3/SrTiO_3$ composites,[15] and $La_{2/3}Ca_{1/3}MnO_3$/alumina composites[16] were reported earlier. Moreover, various films were also grown using different experimental routes, such as partially crystallized $La_{0.5}Sr_{0.5}MnO_3$ film containing amorphous regions as the insulating boundary[17] and epitaxial $La_{0.7}Ca_{0.3}MnO_3/MgO$ nanocomposite film.[18] The latter provided an additional way to control the magnetotransport in manganite films. However, up to now, almost all granular (bulk) composites have been prepared by sintering the mixture of CMR material and insulator powders. But using this method, a higher sintering temperature should be needed for obtaining a good connectivity between two phases. So it is difficult to control and manipulate the interfaces and grain sizes in granular bulk composites. In this paper, we introduce an experimental route, dispersing particle polymer-network gel method, to prepare LCMO/CeO_2 nanocrytalline composites, where CeO_2 is chosen because it is an extremely refractory oxide and nonmagnetic insulating material.

II. EXPERIMENTS

Nanocrystalline LCMO powder with average grain size of 30 nm was first prepared by a polymer-network gel method[19–21] followed by heat treatment. According to the formula $La_{2/3}Ca_{1/3}MnO_3$, stoichiometric amounts of $La(NO_3)_3 \cdot 6H_2O$, $Ca(NO_3)_2$, and $Mn(CHCOO)_2 \cdot 4H_2O$ were dissolved in de-ionized water containing citric acid, forming a uniform solution. After the pH value regulated with ammo-

[a)]Author to whom correspondence should be addressed; electronic mail: rcyu@aphy.iphy.ac.cn

nia, polymerization agents and starters were added to the solution. Keeping the temperature at 80 °C for a few minutes, the solution polymerized into polymer gel. The gel was crushed, dried at 120 °C, and then fired at 500 °C in an oxygen atmosphere to convert the gel into LCMO superfine powder. In order to prepare $LCMO/CeO_2$ composites, the preprepared LCMO powder was firstly cleaned in solution of de-ionized water and alcohol for 24 h. After naturally depositing for 6 h, the upper liquid was poured away and a certain volume of de-ionized water was added again to make the deposition becomes suspension. Then an appropriate stoichiometric amounts of $Ce(NO_3)_3 \cdot 6H_2O$ were dissolved according to different fraction contents of CeO_2 in composites. After that, being dispersed to uniform suspension in ultrasonic cleaner for 30 min, the gelling process is the same as that mentioned above. Finally, the resulting composite powders were sintered at 700 °C for 3 h and cooled down to room temperature to yield bulk products. In our experiments, we have prepared several xLCMO/$(1-x)$$CeO_2$ composites with different metallic (LCMO) fraction contents x (x =100%, 85%, 70%, 60%, 50%, 35%, and 25%).

In order to study microstructures of the composites, transmission electron microscopy (TEM) and high-resolution transmission electron microscopy (HRTEM) experiments were carried out on a Philips CM 12 and Tecnai F20 electron microscopes, respectively. The morphology of the bulk composites was checked with an XL30 S-FEG scanning electron microscope (SEM). Magnetic and electrical properties were measured with MaglabExa Measurement System. The resistivity as a function of temperature was measured using a standard four point technique.

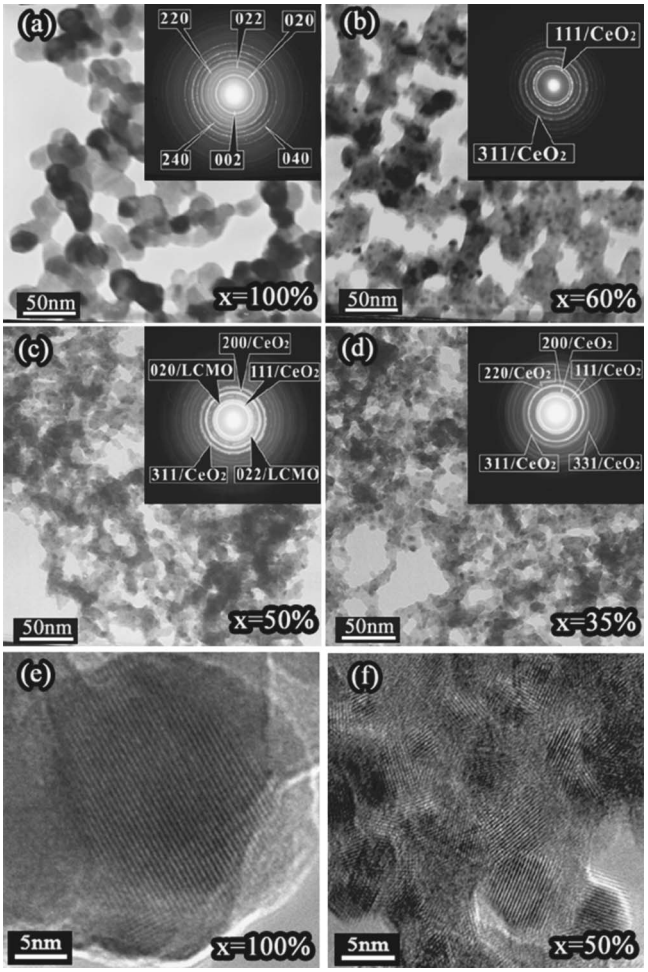

FIG. 1. [(a)-(d)] Electron diffraction patterns from different composites and the corresponding TEM photographs. [(e) and (f)] HRTEM images of x =100% and x=50% */*samples. (e) shows that the average grain size of the LCMO grains is about 30 nm, while (e) shows that some CeO_2 grains of less than 10 nm are formed in the process of preparation.

III. RESULTS AND DISCUSSION

The electron diffraction patterns of the composites are shown in Fig. 1. For pure LCMO powder, all diffraction rings in Fig. 1(a) can be indexed to an orthorhombic structure. With the decrease of x in composites, the diffraction rings of CeO_2 with cubic structure gradually appear from Fig. 1(b) to Fig. 1(d) and the intensities of the diffraction rings become stronger and stronger simultaneously. These results indicate that the $LCMO/CeO_2$ composites have been prepared. In Figs. 1(a)–1(d), TEM images of the powders are also presented from some zones corresponding to the diffraction patterns. It is clearly seen that the grains are very uniform and the average size is about 30 nm for pure LCMO powder. While for the composites, as shown in Figs. 1(b)–1(d), the small grains in relation to CeO_2 adhere to the surface of LCMO grains and have gradually covered LCMO with the increase of CeO_2 content up to x=35%. For comparison of the grain sizes and crystallization of LCMO and CeO_2, Figs. 1(e) and 1(f) show two high-resolution transmission electron microscopy images with distinct features. The smallest size of CeO_2 grains is less than 10 nm in the composites.

Due to high activity of the small grain of CeO_2, it is expected that the composite powders can form bulk products at a relative low sintering temperature such as 700 °C mentioned above. We also carried out SEM observation and found that all the samples have good connectivity, as shown in Fig. 2. Especially, with the introduction of CeO_2 grains, the small CeO_2 grains become bridges to connect LCMO grains, and thus it enhances the compactness of the composites. For the x=35% sample, the configuration of LCMO grains is invisible since it is covered with a large amount of CeO_2 grains with the size of less than 30 nm.

The general behavior of magnetization versus temperature indicates a long-range ferromagnetism below T_C for all composites, and the T_C remains unchanged around 270 K. Here, we only plotted $M(T)$ curves for the x=100% and 35% samples in Fig. 3(a). At low temperature, the existence of spin-glass state was indicated by the measurements of the zero-field-cooled and field-cooled M-T curves. But the inset of Fig. 3(a) shows the reduction of the saturation moment (per weight of LCMO) with decreasing x due to the increase of disorder at the interfaces. This disorder can be viewed as the presence of paramagnetic (PM) grain boundaries from the viewpoint of Ju *et al.*[22]

The resistivities were measured by the standard four-probe method in the range of 5–300 K and in fields up to 5 T. The resistivity versus temperature $\rho(T)$ curves for all samples at zero magnetic field were measured. As expected,

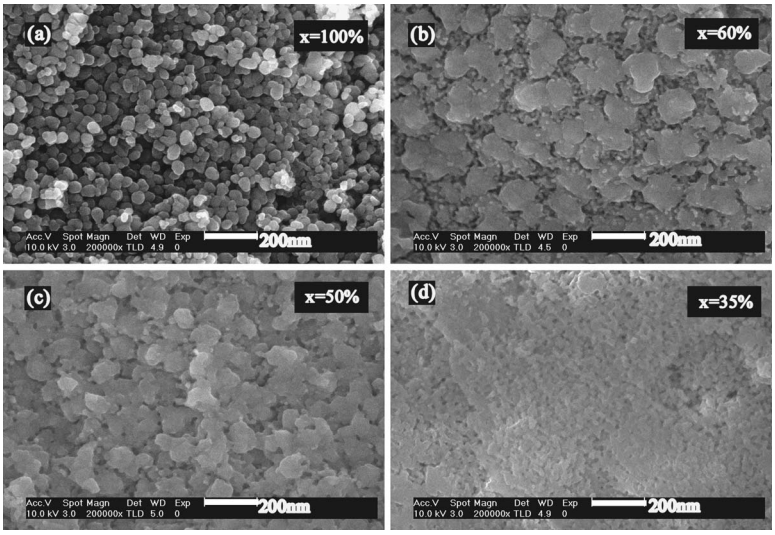

FIG. 2. SEM images of a series of composites.

the resistivity of the composites increases moderately upon the addition of CeO_2 up to $x=60\%$ and then increases rapidly with further increasing CeO_2 content. Compared with pure LCMO sample, the resistivity of the $x=35\%$ sample increases three orders of magnitude at low temperature, so that the metal-insulator transition is completely suppressed by the insulating CeO_2. In the case of $x=25\%$ sample, the resistivity increases six orders of magnitude at room temperature and exceeds the measurement range of the instrument. Here, it should be pointed out that this increase in resistivity and the disappearance of the transition are not due to the doping of CeO_2 inside the LCMO grains, but to the increase in the electron scattering by the insulating CeO_2 grains. In our composites, the metallic percolation threshold x_p is about 35%. As for the conduction behavior with the variation of metallic volume fraction, the relevant literatures reported about metallic percolation threshold, and it is pointed out that the MR reaches a maximum at near x_p.[14] In order to clearly display the variation trend of $\rho(T)$, the normalized resistivity $\rho(T)/\rho(300\ \mathrm{K})$ are depicted in Fig. 3(b), where not only the ratio $\rho(T)/\rho(300\ \mathrm{K})$ increases as metallic volume fraction decreases, but also the maximum $\rho(T_m)$ of resistivity shifts to lower temperatures as the insulating CeO_2 volume fraction increases. The inset of Fig. 3(b) summarizes the variation of T_m with x, which is similar to the behavior in the pure LCMO nanocrystal with decreasing the grain size, namely, the addition of CeO_2 increases the barrier thickness. In addition, according to the relevant reports,[23] the broad peak in the $\rho(T)$ curves can be understood from a two-channel model, that is, the composites consist of parallel network of conducting and insulating paths. However, the microscopic transport mechanisms are unclear yet.

The temperature dependence of the resistivity at different magnetic fields has been measured for our samples. As expected, it is found that the decreases in resistivity are induced by different external magnetic fields for all samples. In Figs. 3(c) and 3(d), two typical $\rho(T)$ curves are shown for the $x=100\%$ and 35% samples. However, it is interesting that the hidden metal-insulator transition appears again at 5 T for

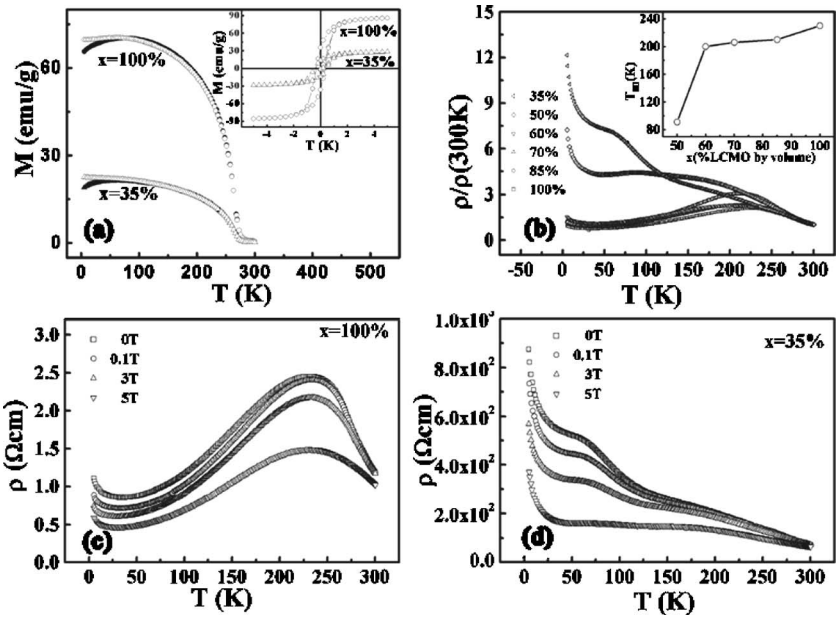

FIG. 3. (a) Magnetization of the $x=100\%$ and 35% samples as a function of temperature after cooling in a zero magnetic field (ZFC) (solid circles and trigons) or in a field of 0.1 T (FC) (open circles and trigons). The inset shows hysteresis loops obtained at 5 K for the $x=100\%$ and 35% samples. (b) Temperature dependence of the normalized resistivity $\rho(T)/\rho(300\ \mathrm{K})$ at zero field. Inset: Temperature (T_m) vs the metallic (LCMO) volume fraction x of the composites, where T_m corresponds to the temperature as $\rho(T)$ reaches a maximum. [(c) and (d)] Temperature dependence of the resistivity $\rho(T)$ at different magnetic fields for the $x=100\%$ and $x=35\%$ samples.

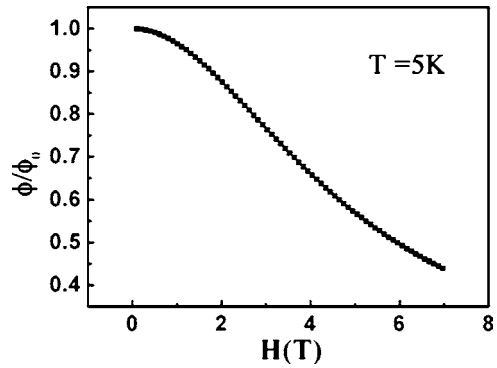

FIG. 4. Magnetic field dependence of barrier height at grain boundaries.

the $x=35\%$ sample since the large magnetic field contributes to spin polarization inside LCMO grains and ferromagnetic coupling among neighboring grains, further reduces the disorders resulting from the addition of CeO_2 grains and the small grain sizes. In other words, the barrier height can be interpreted by the formula:[22] $\phi=\phi_0(1-m_{GB}^2)$, where m_{GB} is the magnetization of PM grain boundary mentioned above and ϕ_0 is the barrier height when $m_{GB}=0$. In addition, according to Langevin function $m_{GB}=\coth(\mu H/K_BT)-K_BT/\mu H$, where μ is the effective magnetic moment of an isolated Mn ion, it is found that the m_{GB} increases with increasing external magnetic field. Thus, the barrier height is effectively decreased under high magnetic fields. In order to clearly display the relationship between ϕ and H, we plotted the ϕ/ϕ_0 vs $H(T)$ curve at 5 K in Fig. 4 on the basis of the two formulas mentioned above [where μ is expressed as $\sqrt{1/3\times\mu_{eff}^2(Mn^{3+})+2/3\times\mu_{eff}^2(Mn^{4+})}$]. Obviously, the large fall in resistivity under high magnetic fields can easily be understood. Figure 3(d) displays the evolution of metal-insulator transition with different magnetic fields. Clearly, the effective decreases in barrier height at high magnetic fields result in a large MR effect. In Fig. 5(a), the MR versus temperature at 5 T is plotted for different samples. Here, high field MR is defined as $-[\rho(H)-\rho(0)]/\rho(0)\times100\%$. The MR value gradually increases with decreasing x and reaches a maximum ($\sim70\%$) at about 50 K and 5 T for $x=x_p\sim35\%$ (see the inset). In the relevant reports,[15,24,25] the MR value for polycrystalline or granular LCMO material is less than 60% under the same measuring conditions.

Besides the high field MR, we also pay attention to MR response at low fields. The MR versus field (MR-H) in the range from −5 to 5 T at 5 K for the series of composites studied is plotted in Fig. 5(b). The MR-H curves show a sharp drop at low fields for all composites followed by a more gradual drop with increasing fields. According to the viewpoints of Balcells *et al.*,[26] the resistivity loops differing from that of bulk samples can be interpreted by the field-induced short-range ferromagnetic correlations among the ferromagnetic particles. In our composites, with the increase of CeO_2 volume fraction, the fall in resistivity becomes steeper at low magnetic fields due to the enhancement of grain boundaries. Generally, low field MR is defined as $-[\rho(H)-\rho(H_C)]/\rho(H_C)\times100\%$, where H_C is the coercive field. For the $x=35\%$ sample, the MR is close to 16% at 5 K and 0.05 T, which is higher than the MR value[10,11] ($\sim9\%$)

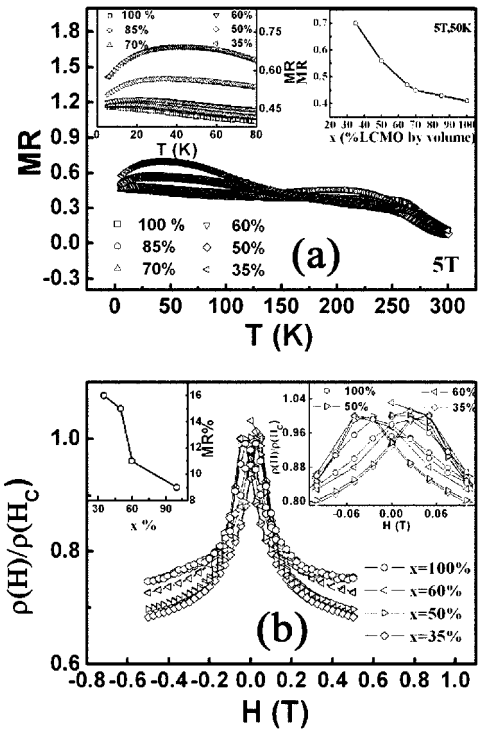

FIG. 5. (a) High field MR ($-[\rho(H)-\rho(0)]/\rho(0)\times100\%$) of all composites vs temperature for different metallic (LCMO) volume fraction x. Left inset: the partial enlarged figure. Right inset: the variation of MR value with increasing x in a 5 T field at 50 K. (b) Low field dependence of resistance $\rho(H)/\rho(H_C)$ of several composites recorded at 5 K. Right inset: the partial enlarged figure, left inset: the variation of MR ($-[\rho(H)-\rho(H_C)]/\rho(H_C)\times100\%$) value with increasing x in a 0.05 T field at 5 K.

of granular LCMO under the same measuring conditions. Moreover, compared with other LCMO/insulator composites with low field MR, such as LCMO/$SrTiO_3$ ($\sim6\%$) (Ref. 15) and LCMO/alumina (less than 10%),[16] our composites show larger MR value ($\sim16\%$) since the smaller grain sizes and good connectivity among neighboring grains in our composites play important roles in enhancing the low field MR.

IV. CONCLUSIONS

In our experiments, we prepared $x La_{2/3}Ca_{1/3}MnO_3/(1-x)CeO_2$ nanocystalline composites by means of a dispersing particle polymer-network gel method. This method will play an important role in preparing relevant nanocrystalline composites. In the series of our sintered composites, it is shown from $\rho(T)$ curves that the metallic percolation threshold is at about $x=x_p\sim35\%$. In addition, we observed the evolution from insulating to metallic behavior induced by large magnetic field for the $x=35\%$ sample. Through the study of the high and low field MR response for all composites, the addition of CeO_2 indeed enhances the field sensitivity of MR, especially at near $x=x_p$.

ACKNOWLEDGMENTS

This work was supported by the National Natural Science Foundation of China (Grant Nos. 50471053, 50321101, and 50332020) and the State Key Development Program for Basic Research of China (Grant Nos. 2005CB623602 and 2005CB724402).

[1]R. M. Kusters, J. Singleton, D. A. Keen, R. McGreevy, and W. Hayes, Physica B **155**, 362 (1989).
[2]R. von Helmolt, J. Wecker, B. Holzapfel, L. Schultz, and K. Samwer, Phys. Rev. Lett. **71**, 2331 (1993).
[3]K. Chahara, T. Ohno, M. Kasai, and Y. Kozono, Appl. Phys. Lett. **63**, 1990 (1993).
[4]A. Urushibara, Y. Moritomo, T. Arima, A. Asamitsu, G. Kido, and Y. Tokura, Phys. Rev. B **51**, 14103 (1995).
[5]J. Z. Liu, I. C. Chang, S. Irons, P. Klavins, R. N. Shelton, K. Song, and S. R. Wasserman, Appl. Phys. Lett. **66**, 3218 (1995).
[6]H. Y. Hwang, S.-W. Cheong, N. P. Ong, and B. Batlogg, Phys. Rev. Lett. **77**, 2041 (1996).
[7]W. E. Picket and D. J. Singh, Phys. Rev. B **53**, 1146 (1996).
[8]M. Ziese, Rep. Prog. Phys. **65**, 143 (2002).
[9]J. H. Park, E. Vescovo, H. J. Kim, C. Kwon, R. Ramesh, and T. Venkatesan, Nature (London) **392**, 794 (1998).
[10]R. D. Sánchez, J. Rivas, C. Vázquez-Vázquez, A. López-Quintela, M. T. Causa, M. Tovar, and S. Oseroff, Appl. Phys. Lett. **68**, 134 (1996).
[11]L. E. Hueso, J. Rivas, F. Rivadulla, and M. A. López-Quintela, J. Appl. Phys. **86**, 3881 (1999).
[12]J. Z. Sun *et al.*, Appl. Phys. Lett. **69**, 3266 (1996).
[13]C. Kwon, Q. X. Jia, Y. Fan, M. F. Hundley, D. W. Reagor, J. Y. Coulter, and D. E. Peterson, Appl. Phys. Lett. **72**, 486 (1998).
[14]S. Gupta, R. Ranjit, C. Mitra, P. Raychaudhuri, and R. Pinto, Appl. Phys. Lett. **78**, 362 (2001).
[15]D. K. Petrov, L. Krusin-Elbaum, J. Z. Sun, C. Field, and P. R. Duncombe, Appl. Phys. Lett. **75**, 995 (1999).
[16]L. E. Hueso, J. Rivas, F. Rivadulla, and M. A. López-Quintela, J. Appl. Phys. **89**, 1746 (2001).
[17]J. M. Liu *et al.*, Appl. Phys. Lett. **76**, 2286 (2000).
[18]V. Moshnyaga *et al.*, Nat. Mater. **2**, 247 (2003).
[19]W. B. Yelon, Z. Hu, W. J. James, and G. K. Marasinger, J. Appl. Phys. **79**, 5939 (1996).
[20]H. W. Zhang, S. Y. Zhang, B. G. Shen, and C. Lin, J. Appl. Phys. **85**, 4660 (1999).
[21]J. H. Lin, S. F. Liu, X. L. Qian, and M. Z. Su, J. Alloys Compd. **238**, 113 (1996).
[22]S. Ju, K. W. Yu, and Z. Y. Li, Phys. Rev. B **71** 224401 (2005).
[23]A. de Andres, M. Garcia-Hernandez, and J. L. Martinez, Phys. Rev. B **60**, 7328 (1999).
[24]R. Shreekala *et al.*, Appl. Phys. Lett. **716**, 282 (1997).
[25]S. L. Yuan *et al.*, Solid State Commun. **125**, 11 (2003).
[26]Ll. Balcells, A. E. Carrillo, B. Martinez, and J. Fontcuberta, Appl. Phys. Lett. **74**, 4014 (1999).